

Article

# Crystal ZnGeP<sub>2</sub> for Nonlinear Frequency Conversion: Physical Parameters, Phase-Matching and Nonlinear Properties: Revision

Sergey G. Grechin <sup>1,\*</sup> and Ilyia A. Muravev <sup>2</sup><sup>1</sup> Prokhorov General Physics Institute of the Russian Academy of Sciences, 119991 Moscow, Russia<sup>2</sup> Informatics, Artificial Intelligence and Control Systems (IU), Bauman Moscow State Technical University, 105005 Moscow, Russia; bauman@bmstu.ru

\* Correspondence: grechinsg@kapella.gpi.ru

**Abstract:** The article presents a comparative analysis of published data for the physical parameters of the ZGP (ZnGeP<sub>2</sub>) crystal, its nonlinear and phase-matching properties, and functional capabilities for all frequency conversion processes (harmonics, sum and difference frequencies, and parametric generation). At the first time, the possibilities for obtaining the temperature-noncritical processes for some combinations of wavelengths are shown.

**Keywords:** ZGP crystal; physical parameters; sum- and difference-frequency conversion; optical parametric oscillation; function capabilities; temperature non-critical processes

## 1. Introduction

Mid-infrared (IR) radiation is widely used for solving different tasks [1–3]. These are spectroscopy [4], medicine (diagnostic, therapy, surgery) [5], analysis of biological systems [6–8], monitoring of trace gases and remote sensing [9–11], preservation of historical values [12–14], ecological studying of soil [15], etc. A large number of applications are based on methods of spectroscopy with different wavelengths of radiation. For forming these, nonlinear optical frequency conversion of laser radiation is used. The generation of the sum and difference of the frequencies makes it possible to generate radiation at fixed wavelengths. The wavelength variation in a wide range is provided by an optical parametric oscillator (OPO) [16–18]. Currently, sources have been developed for generation radiation in both continuous and pulsed mode (from monopulse to femtosecond durations of pulses).

Commercially produced crystals are widely used for nonlinear optical frequency conversion: AGS (AgGaS<sub>2</sub>), AGSe (AgGaSe<sub>2</sub>) and ZGP (ZnGeP<sub>2</sub>) [19,20]. Crystal ZGP stands out among them. It has important advantages—a large range of transparency, large values of effective nonlinearity coefficient and thermal conductivity, an optimal birefringence value, a sufficiently high damage threshold, etc. The synthesis and research of ZGP began in the “semiconductor era”. The results of the work of this period are given in [21]. The possibility for application of this crystal for nonlinear optical frequency conversion was obviously shown for the first time in the article [22]. In the past, a large number of studies of its physical properties have been carried out, and various frequency conversion processes with various schemes of solutions have been implemented.

This paper provides an overview of the published data on the physical parameters of the ZGP crystal, and its phase-matching properties for various tasks of nonlinear optical frequency conversion (harmonic generation, sum and difference frequencies, and parametric generation). Many of the data on ZGP properties published before 2005 are given in the well-known D. Nikogosyan handbook [23]. More complete data are given in [24].



**Citation:** Grechin, S.G.; Muravev, I.A. Crystal ZnGeP<sub>2</sub> for Nonlinear Frequency Conversion: Physical Parameters, Phase-Matching and Nonlinear Properties: Revision. *Photonics* **2024**, *11*, 450. <https://doi.org/10.3390/photonics11050450>

Received: 5 March 2024

Revised: 23 April 2024

Accepted: 24 April 2024

Published: 11 May 2024



**Copyright:** © 2024 by the authors. Licensee MDPI, Basel, Switzerland. This article is an open access article distributed under the terms and conditions of the Creative Commons Attribution (CC BY) license (<https://creativecommons.org/licenses/by/4.0/>).

## 2. Physical Parameters of the ZGP Crystal

The positive uniaxial crystal ZGP belongs to the  $\bar{4}2m$  point symmetry group. In general, crystal growth is carried out by the Bridgman–Stockbarger technique. The lattice parameters, all thermo-physical parameters, and the transparency range were determined fairly accurately at the initial stage of research into its properties [23,24].

The first measurement of the nonlinear susceptibility tensor coefficient was executed in [22] when it was compared with GaAs. The value  $d_{14} = d_{25} = d_{36} = 111$  pm/V was obtained. For a ZGP crystal grown by the encapsulated Czochralski method [25], the value of  $d_{36} = 50$  pm/V. The reasons for such a small value are not specified by the authors.

In subsequent years, the value of  $d_{36}$  was clarified, and it is now accepted that for crystals grown using Bridgman technology,  $d_{36} = 75$  pm/V [26] (the question about the dispersion of the  $d_{36}$  coefficient and its dependence versus temperature is not considered here, although it can be expected that it will be no less than in oxide crystals [27]). In any case, for the point group  $\bar{4}2m$ , the distribution of the effective nonlinearity coefficient  $d_{\text{eff}}(\varphi, \theta)$  is determined by a single coefficient  $d_{36}$ , and its form, for different values of the coefficients of the tensor  $d_{ij}$ , will be similar. The  $d_{\text{eff}}(\varphi, \theta)$  distributions for the two types of interaction are shown in Figure 1. The dark red areas correspond to the maximum values of  $d_{\text{eff}}$ , and the black ones correspond to zero values. The white line on Figure 1 shows the directions of phase matching for generation of the third harmonic at a wavelength of 10.6  $\mu\text{m}$ . It follows from the results of Figure 1 that for the *eeo* type of phase matching, an angle-noncritical process is possible (at  $\theta_{\text{pm}} = 90^\circ$ ). Principally, this cut allows for the realization of the maximum efficiency of radiation conversion with high divergence, but at the same time, for *eeo* interaction  $d_{\text{eff}}(0^\circ, 90^\circ) = 0$ . This mode is possible for *oeo* type with a maximum value of  $d_{\text{eff}}(45^\circ, 90^\circ) = d_{36}$ .

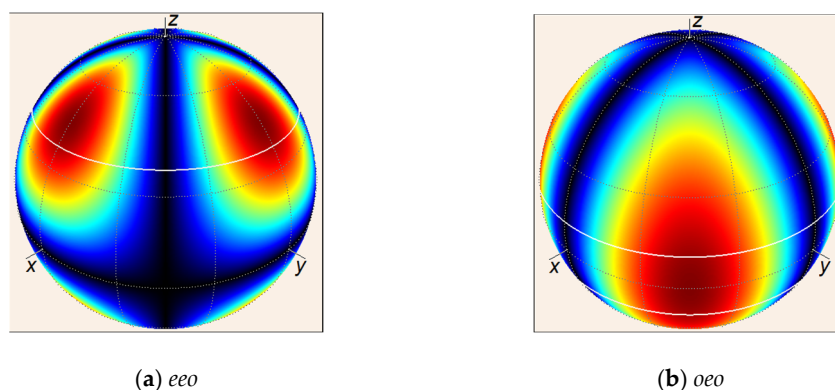
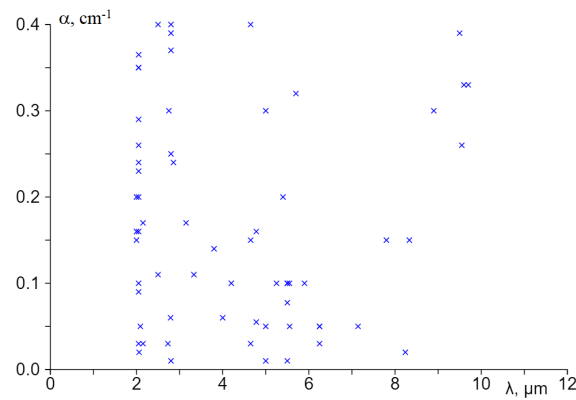


Figure 1. Distribution of  $d_{\text{eff}}(\theta, \varphi)$  for two types of interactions.

The crystal transparency range is 0.74–12  $\mu\text{m}$  [23,24]. A distinctive feature of ZGP is that in the local region with a wavelength of 9.0  $\mu\text{m}$ , the effect of multi-phonon absorption is manifested, which leads to an increase of the total losses in this wavelength range (see [24]).

In the first works, the ZGP crystal was distinguished by a large loss value (in the transparency band up to 6  $\text{cm}^{-1}$ ). Pumping at the radiation wavelength of widely used  $\text{Nd}^{3+}$  lasers at 1.06  $\mu\text{m}$  is practical interest for creating OPO with a large wavelength tuning range. But the pumping wavelength is at the boundary of the transparency range, and the coefficient of losses at this wavelength is 0.75–5.6  $\text{cm}^{-1}$ . Currently, radiation in the range of 2.0–3.0  $\mu\text{m}$  is widely used for pumping OPO [16–20]. This is optimal for many tasks in terms of obtaining the required tuning range and ensuring the conversion process with minimal losses. The development of growth technology and post-growth treatment made it possible to reduce the value of the absorption coefficient in the range of 2–8  $\mu\text{m}$  to 0.01–0.02  $\text{cm}^{-1}$  [28–31]. Figure 2 shows the values of absorption coefficients of no more than 0.4  $\text{cm}^{-1}$  at various wavelengths from different publications [24]. (The bibliographic references for the data in Figure 1 are given in [24]). For crystals grown in recent years, the

difference in the values of the absorption coefficient can reach 10 or more times. This is obviously due to the technology of growing and post-growth processing of crystals. This is not disclosed in the publications.



**Figure 2.** The values of absorption  $\alpha(\lambda)$  at different wavelengths.

An important parameter is the value of the crystal laser-induced damage threshold. In this work, we do not provide data, since a detailed description of the obtained values and methods for increasing the damage threshold are given in [32,33].

Phase matching, which determines the possibility of effective frequency conversion, is determined by the main values of the refractive indices  $n_i(\lambda)$ . The first results of  $n_i(\lambda)$  measurements in the entire ZGP transparency range were given in [22]. The Sellmeier equations obtained on the basis of data from [22] were published in [34]. From 1976 to 2023, the Sellmeier equations for ZGP at various temperatures are given in 17 articles [34–50]. The dependences of  $n_i(\lambda)$  on the data from these studies at room temperature, obtained using [24], are shown in Figure 3 (the dotted lines show the boundaries of applicability for the equation). Such a number of equations for  $n_i(\lambda)$  is due to the fact that there were significant differences between the results of measurements and calculations for phase-matching angles (see, for example, [35,37,42,46,51,52]). The differences in the angles reached  $15^\circ$ – $20^\circ$ . Many authors attribute this to the error in determining refractive indices, which, according to their estimates, ranges from 0.001 to 0.004. In some studies, it was noted that for crystals with different values of absorption coefficients the refractive indices have equal values. But the full expression for refractive indices also takes into account the loss of the medium [19,20]. These losses should influence on the value of the refractive indices. Detailed studies in the mid-IR range have not been conducted at present.

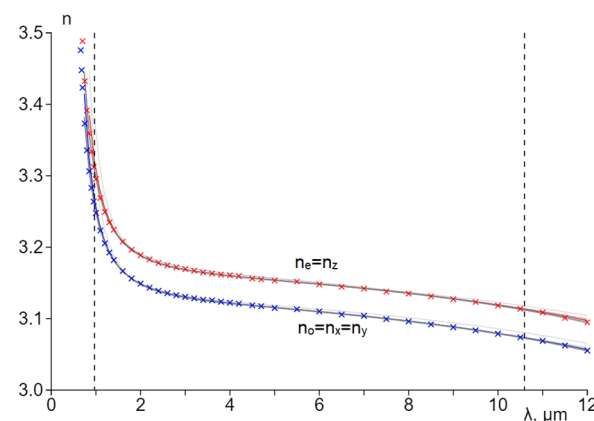


**Figure 3.** The dispersion of  $n_i(\lambda)$  for ZGP crystal.

The ZGP crystal is widely used in optical parametric oscillators. The refinement of the Sellmeier equations coefficients is based on a comparison of the experimentally obtained

tunable characteristics of the OPO with the calculated ones. But the generation process in OPO occurs in the mode of a strong energy exchange (not in the fixed field approximation), with the contribution of coupled nonlinear processes [53–61]. The obtained Sellmeier equations are, in fact, “technical” characteristics corresponding to a certain mode of the generation process. They are important, but they cannot always be used for other generation processes in OPO and other schemes solutions.

The articles for the ZGP crystal use Sellmeier equations of various types. All of them can be reduced to the following one- and two-resonant forms (electron- and phonon-resonant wavelengths on the transparency range boundaries)

$$n_i^2 = A_i + \frac{B_i\lambda^2}{\lambda^2 - C_i} + \frac{D_i\lambda^2}{\lambda^2 - E_i} = A_i + \frac{B_i\lambda^2}{\lambda^2 - \lambda_{e,i}^2} + \frac{D_i\lambda^2}{\lambda^2 - \lambda_{p,i}^2} \tag{1}$$

$$n_i^2 = A_i + \frac{B_i\lambda^2}{\lambda^2 - C_i} + D_i\lambda^2 = A_i + \frac{B_i\lambda^2}{\lambda^2 - \lambda_{e,i}^2} + D_i\lambda^2 \tag{2}$$

In these expressions, the free terms  $C_i$  and  $E_i$  determine the resonant wavelengths of the electron ( $\lambda_{e,i}$ ) and phonon ( $\lambda_{p,i}$ ) absorption spectra.

Table 1 shows the values of refractive indices, birefringence ( $n_z - n_x$ ) at a wavelength of 10  $\mu\text{m}$ , wavelengths  $\lambda_{e,i}$  and  $\lambda_{p,i}$ , and differences between the maximum and minimum values of the parameters (max–min). The values of  $\lambda_{p,i}$  are not given when using single-resonance Sellmeier equations of the form (2). The maximum differences for refractive indices are the following: for  $n_o = n_x = 0.00855$ , and for  $n_e = n_z = 0.01045$ . The biggest difference is for  $n_e = n_z$ . The value of the wavelength  $\lambda_{e,i}$  is poorly consistent with the magnitude of the band gap. There are big differences for  $\lambda_{p,i}$ . If this is due to the quality of the crystal (for example, the presence of impurities), appropriate clarifications are needed. It is also necessary to clarify the values of the intensity, pulse duration and average radiation power with which the measurements were carried out.

**Table 1.** Optical parameters of ZGP crystal at wavelength 10  $\mu\text{m}$ .

| T, K    | $n_o = n_x$ | $n_e = n_z$ | $n_z - n_x$ | $\lambda_{e,x}, \mu\text{m}$ | $\lambda_{e,z}, \mu\text{m}$ | $\lambda_{p,x}, \mu\text{m}$ | $\lambda_{p,z}, \mu\text{m}$ | Ref. |
|---------|-------------|-------------|-------------|------------------------------|------------------------------|------------------------------|------------------------------|------|
| 293     | 3.07899     | 3.11816     | 0.03918     | 0.3665                       | 0.3782                       | 27.39                        | 27.38                        | [34] |
| 293     | 3.07914     | 3.11831     | 0.03916     | 0.3658                       | 0.3776                       | 25.74                        | 25.74                        | [35] |
| 373     | 3.08019     | 3.11927     | 0.03908     | 0.3709                       | 0.3821                       | 25.74                        | 25.74                        | [36] |
| 293     | 3.07914     | 3.1183      | 0.03916     | 0.3658                       | 0.3776                       | 25.74                        | 25.74                        | [50] |
| 293     | 3.07857     | 3.11995     | 0.04138     | 0.3419                       | 0.3913                       |                              |                              | [37] |
| 293     | 3.07878     | 3.11821     | 0.03943     | 0.3691                       | 0.3787                       | 30                           | 30                           | [38] |
| 293     | 3.07851     | 3.11819     | 0.03968     | 0.3659                       | 0.3793                       | 40.67                        | 31.64                        | [39] |
| 293     | 3.07938     | 3.11963     | 0.04025     | 0.3419                       | 0.3913                       |                              |                              | [40] |
| 293     | 3.07889     | 3.11234     | 0.03345     | 0.3655                       | 0.3773                       |                              |                              | [41] |
| 293     | 3.07929     | 3.11878     | 0.03949     | 0.6389                       | 0.6439                       | 24.72                        | 21.26                        | [42] |
| 293     | 3.07957     | 3.11912     | 0.03955     | 0.4687                       | 0.4681                       | 28.86                        | 30.84                        | [43] |
| 293     | 3.08582     | 3.12278     | 0.03696     | 0.3992                       | 0.3537                       | 30                           | 30                           | [44] |
| 293     | 3.07957     | 3.11912     | 0.03954     | 0.4289                       | 0.4681                       | 28.86                        | 30.84                        | [46] |
| 293     | 3.07901     | 3.11778     | 0.03876     | 0.3605                       | 0.3742                       | 25.74                        | 25.74                        | [48] |
| 293     | 3.079       | 3.11739     | 0.03839     | 0.3937                       | 0.3673                       | 26.58                        | 24.57                        | [47] |
| 293     | 3.07727     | 3.1166      | 0.03933     | 0.3685                       | 0.3813                       | 30                           | 30                           | [49] |
| max-min | 0.00855     | 0.01045     | 0.00794     | 0.297                        | 0.2902                       | 15.95                        | 9.58                         |      |

For *eeo* type of interaction, the phase-matching angle for second harmonic generation (SHG) process is determined by the following expression, which shows the significant role of the birefringence values  $n_{2o} - n_{1o}$  and  $n_{1e} - n_{1o}$  (index 1 corresponds to fundamental radiation, 2 to the second harmonic):

$$\theta_{pm} = \arcsin\left(\frac{n_{1e}}{n_{2o}} \sqrt{\frac{(n_{2o} - n_{1o})(n_{2o} + n_{1o})}{(n_{1e} - n_{1o})(n_{1e} + n_{1o})}}\right) \quad (3)$$

The differences in expression (3) show that small errors in determining the values of the refractive indices lead to large errors in the phase-matching angles.

The values of the  $n_{1e} - n_{1o}$  are significantly different in various publications at the boundaries of the crystal transparency range (at 10  $\mu\text{m}$ , see Table 1). This leads to a large difference in the phase-matching angles both for the different harmonic generation, the sum and different wave processes, and for the parametric oscillators.

Figure 4 shows the dependences of the phase-matching angles for the second harmonic generation with the *eeo* type of interaction in the crystal transparency range, obtained with various Sellmeier equations from [24]. In the wavelength range of the fundamental radiation of about 4–6  $\mu\text{m}$ , the difference in the values of the phase-matching angles does not exceed several degrees. They have unacceptably large values at the boundaries of the range (up to 15°–20°).

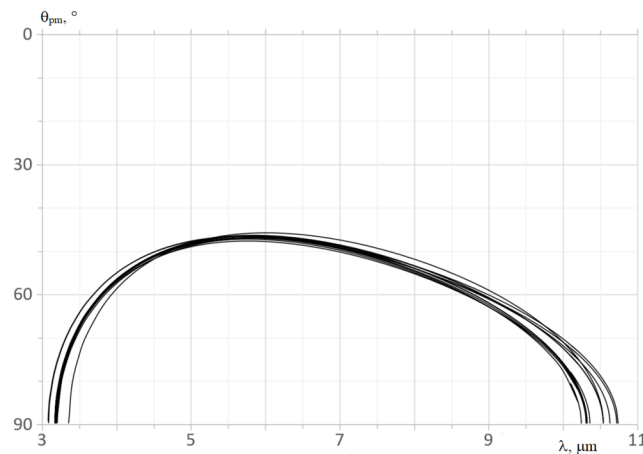
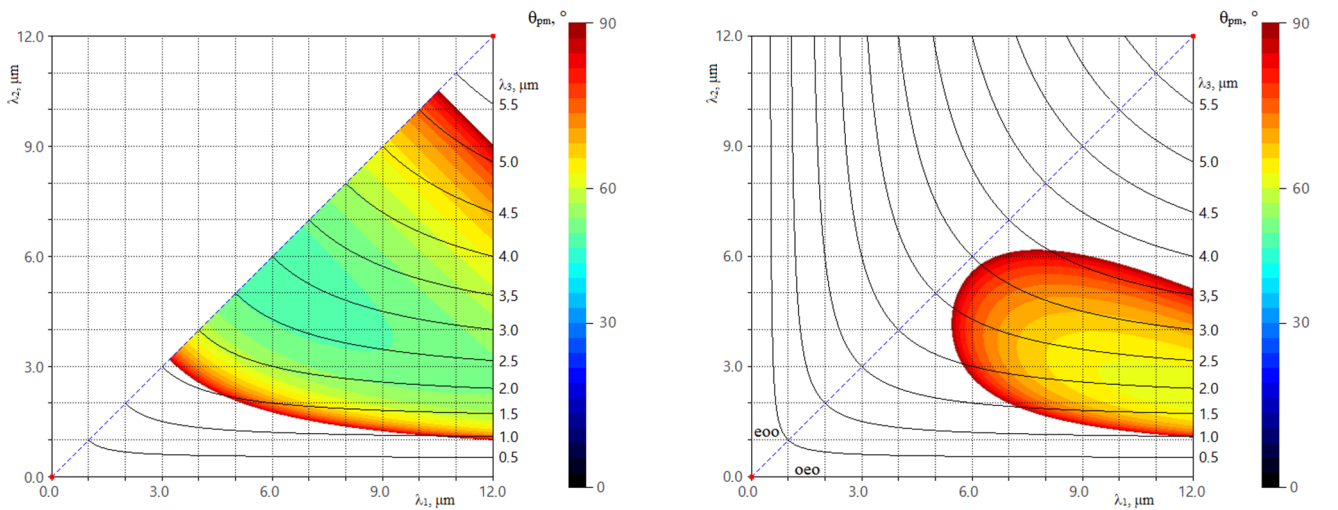


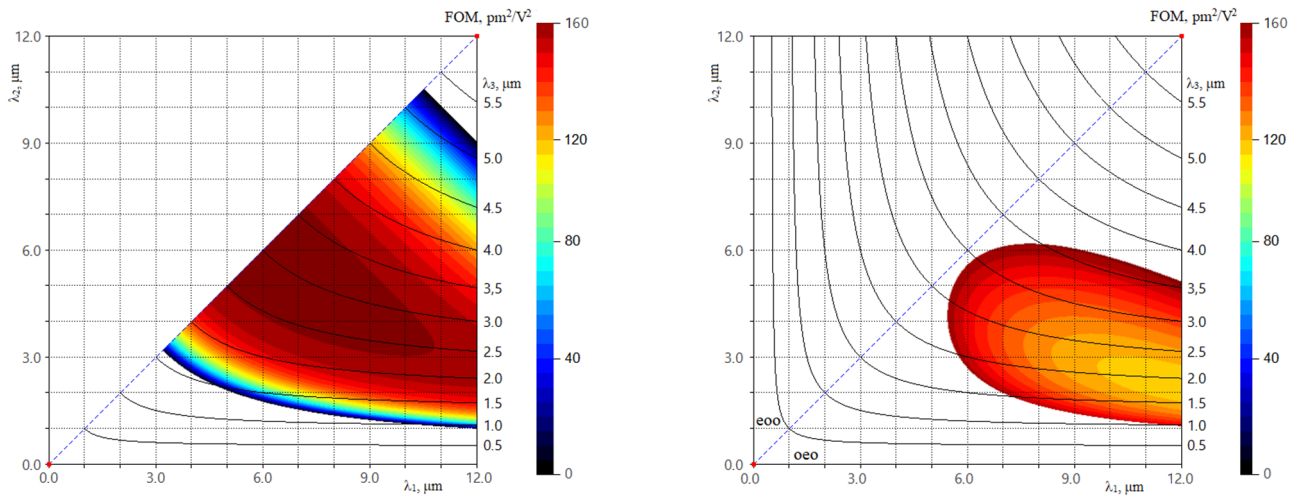
Figure 4. Angle of phase matching for SHG versus wavelength for *eeo* type of interaction.

### 3. Function Capabilities of ZGP Crystal for Frequency Conversion

It is convenient to represent the crystal function capabilities for all frequency conversion processes in the form of distributions that was proposed in [62]. Figure 5 shows the distributions of the phase-matching angles  $\theta_{pm}(\lambda_1, \lambda_2)$  and the figure of optical merit FOM ( $FOM(\lambda_1, \lambda_2) = d_{\text{eff}}^2(\varphi_{pm}, \theta_{pm}) / n_1 n_2 n_3$ ) in the crystal transparency range for two types of interaction (*eeo* and *oeo*) depending on the wavelengths  $\lambda_1$  and  $\lambda_2$ . The calculations were executed with the application of the Sellmeier equations from [46]. Calculations of FOM are executed along the directions of phase matching  $\theta_{pm}$  at the optimal value of the angle  $\varphi_{pm}$ . The isolines of the distributions in Figure 5 correspond to some fixed values of the phase-matching angles and FOM, the scales of values for which are shown to the right of the distributions. The bisector of the distribution corresponds to the second harmonic generation ( $\lambda_1 = \lambda_2$ ). The oblique dotted line corresponds to one of the special cases—the generation of the third harmonic. The black lines on the distributions show wavelength values  $\lambda_3 (\lambda_3 = (1/\lambda_1 + 1/\lambda_2)^{-1})$ .



(a) Phase-matching angles



(b) Figure of Optical Merit

*eeo*

*oeo*

**Figure 5.** Results for  $\theta_{pm}(\lambda_1, \lambda_2)$  (a) and  $FOM(\lambda_1, \lambda_2)$  (b) with data for  $n(\lambda_1, \lambda_2)$  from [46].

All values of  $\theta_{pm}$  and FOM for different combinations of wavelengths  $\lambda_1$  and  $\lambda_2$  correspond to the case of sum-frequencies generation and different harmonics. The results of Figure 5 along curves with fixed values of  $\lambda_3$  allow us to determine combinations of wavelengths  $\lambda_1$ ,  $\lambda_2$ , and values of  $\theta_{pm}$  and FOM, which can be obtained for parametric generation. Changing the phase-matching angle along curves with fixed values of  $\lambda_3$  allows to determine the range of angular tuning. Also, the distributions in Figure 5 allow us to determine the frequency tuning range for a parametric generator with a fixed value of the cutoff angle—along the corresponding line for the angle  $\theta_{pm}$ .

The small value of birefringence  $\Delta n = n_z - n_x$  of the main indices of refraction leads to the fact that all frequency conversion processes are possible only for the first type of phase matching, *eeo*. For the *oeo* type of phase matching, the SHG process is impossible, but sum- and difference-frequency generation, and parametric generation can be obtained. On the other hand, a small value of  $\Delta n$  gives a large value of the angular bandwidth of the phase matching.

The boundary of the distribution  $\theta_{pm}(\lambda_1, \lambda_2)$  for the phase-matching angles (Figure 5a) corresponds to the case  $\theta_{pm} = 90^\circ$ . A comparison of these results with the FOM distribution (Figure 5b) shows, as noted above (Figure 1), that angular non-critical phase matching is possible for *eeo* and *oeo*, but for the *eeo* type of interaction the value for FOM = 0. When generating the sum frequency for two types of interaction, the minimum wavelength of  $\lambda_3$  (up to 0.7  $\mu\text{m}$ ) can be obtained not with SHG, but with the generation of the sum frequencies. With parametric generation, the maximum wavelength tuning range for  $\lambda_1$  can be obtained for the *eeo* type of phase matching when pumped at a wavelength  $\lambda_3 = 2.0\text{--}2.1 \mu\text{m}$ . The potential tunability range is  $\lambda_1 = 4\text{--}12 \mu\text{m}$  in this case. In the shortwave part of the tuning range, the FOM value is not very important. But it increases significantly in the longwave part of the range. This creates prerequisites for increasing the conversion efficiency, since the effective gain per pass is inversely proportional to the wavelength of the generated radiation. It is possible to obtain a much larger FOM value when pumping at a wavelength of  $\lambda_3 = 2.5\text{--}3.0 \mu\text{m}$ . But the minimum value of the wavelength for  $\lambda_1$  in this case is 5–6  $\mu\text{m}$ .

For OPO results for the  $\theta_{pm}$  distribution, it is convenient to represent them depending on  $\lambda_1$  and  $\lambda_3\text{--}\theta_{pm}(\lambda_1, \lambda_3)$ . For the *eeo* type of interaction this distribution is shown in Figure 6a. The horizontal dotted line is set to  $\lambda_3 = 2.7 \mu\text{m}$ . Figure 6b shows the dependencies  $\theta_{pm}(\lambda_1)$  and FOM( $\lambda_1$ ) corresponding to this value of  $\lambda_3 = 2.7 \mu\text{m}$ . Table 2 shows the values of the main parameters at the boundaries of the tunability range (Left and Right). For the above special case of pumping with  $\lambda_3 = 2.7 \mu\text{m}$ , the tuning at a wavelength of  $\lambda_1$  in the range of 5.4–12  $\mu\text{m}$  is performed when the phase-matching angle changes from  $46.7^\circ$  to  $51^\circ$  (by  $4.3^\circ$ , recall that the crystal tuning angle will be greater by the value of the refractive index). The total wavelength range of the output radiation ( $\lambda_1$  and  $\lambda_2$ ) will be 3.45–12  $\mu\text{m}$ .

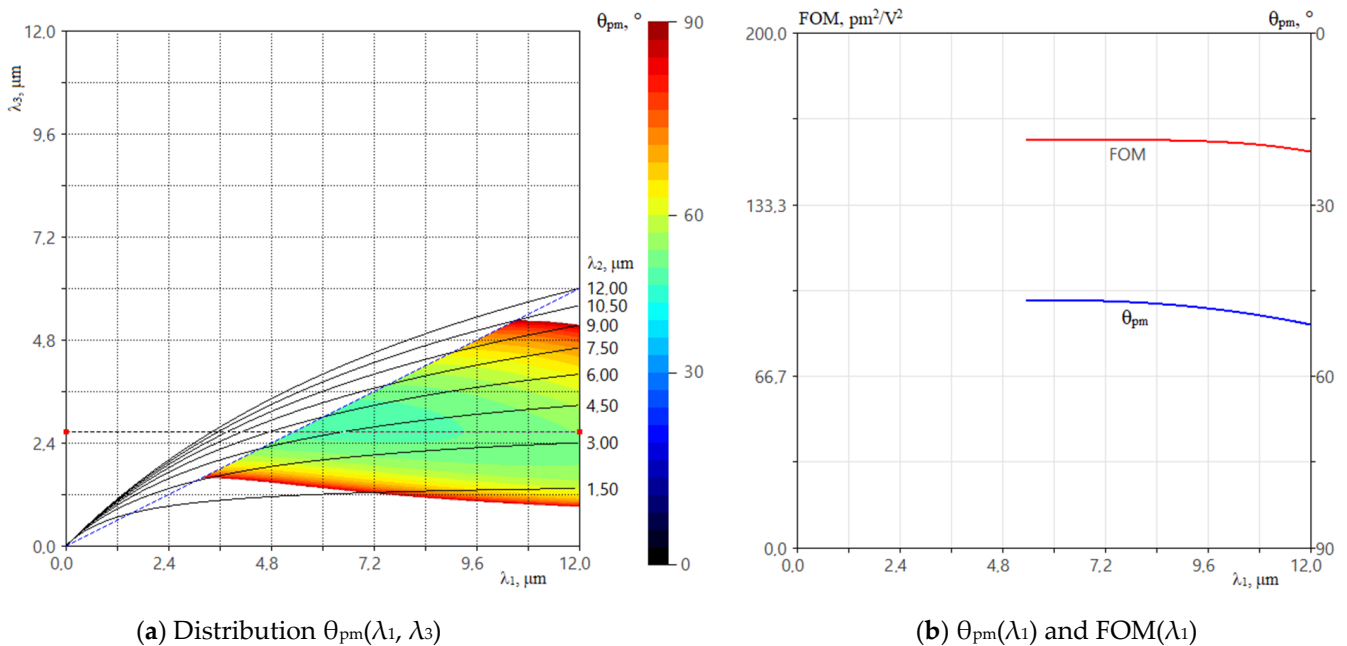


**Figure 6.** Distributions: (a)  $\theta_{pm}(\lambda_1, \lambda_3)$ , and (b)  $\theta_{pm}(\lambda_1)$  and FOM( $\lambda_1$ ) at  $\lambda_3 = 2.7 \mu\text{m}$ .

It should be noted that, when pumped at a wavelength of  $\lambda_3 = 2.7 \mu\text{m}$  (Figure 6b) in the range  $\lambda_1 = 5.3\text{--}6.8 \mu\text{m}$ , the phase-matching angle  $\theta_{pm} = 46.8^\circ$  with the *eeo* type of interaction practically does not change. This corresponds to the possibility of forming a broadband radiation at  $\lambda_1$  with a narrowband pump radiation at  $\lambda_3$ . In Figure 6a, this corresponds to the fact that the horizontal dotted line  $\lambda_3 = 2.7 \mu\text{m}$  is tangent to the isolines of the distribution of the phase-matching angle  $\theta_{pm}$ . This mode is possible in the wavelength range  $\lambda_3 = 2.4\text{--}3.0 \mu\text{m}$ . But at the edges of the wavelength range  $\lambda_3$ , the width of the spectrum at wavelength  $\lambda_1$  decreases.

**Table 2.** Values of parameters for OPO at  $\lambda_3 = 2.7 \mu\text{m}$ .

|                               | Left  | Right |
|-------------------------------|-------|-------|
| $\lambda_1, \mu\text{m}$      | 5.4   | 12.0  |
| $\lambda_2, \mu\text{m}$      | 5.4   | 3.45  |
| $\lambda_3, \mu\text{m}$      | 2.7   | 2.7   |
| FOM, $\text{pm}^2/\text{V}^2$ | 198.7 | 154.2 |
| $\theta, ^\circ\lambda$       | 46.7  | 51.0  |
| $\varphi, ^\circ$             | 0     | 0     |

For the *o eo* type of interaction for parametric generation the maximum tuning range in the range of 5.5–12  $\mu\text{m}$  at a wavelength of  $\lambda_1$  can be obtained when pumped at a wavelength of 2.7  $\mu\text{m}$ . But the value of the FOM is much smaller.

With other Sellmeier equations in calculations there are small quantitative changes in the results, but the overall picture does not change qualitatively.

#### 4. Thermo-Optical Parameters of ZGP Crystal for Frequency Conversion

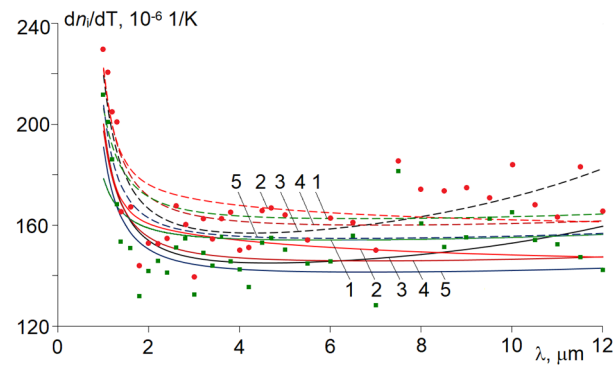
The temperature width of the phase matching and the possibility of temperature tunability of the wavelength in OPO are determined by the temperature derivatives  $dn_i(\lambda)/dT$  for the main values of the refractive indices. The first measurements of  $dn_i(\lambda)/dT$  in the crystal transparency range were published in [22]. But very large differences in measured values were obtained (see below).

In most cases, the Sellmeier equations are given independently for refractive indices at room temperature  $n_i(\lambda)$  [34,35,37–44,46,48,50] and for expressions for first-order derivatives  $dn_i(\lambda)/dT$  [35,36,43,63], depending on the wavelength. In recent years, the Sellmeier equations have been given with temperature-dependent coefficients [36,47,49,50]. The temperature dependence of coefficients are given in Equations (1) and (2) by the Taylor series from the first to the third orders. This allows us to take into account the high-order nonlinear dependence of the refractive index versus temperature. Also, in [35,36,38], the Sellmeier equations with fixed values of coefficients in (1) and (2) at different temperatures are given. In most cases, the temperature range is quite large.

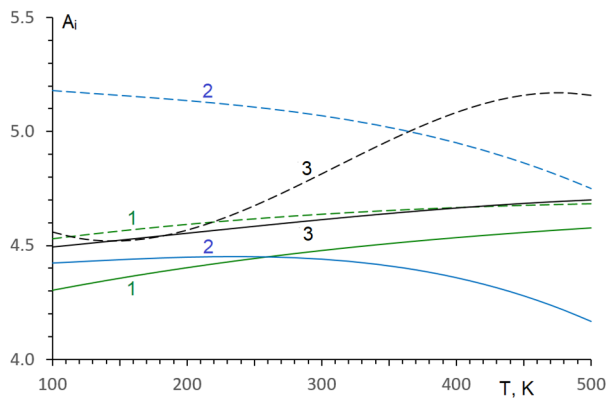
In [63], a semi-empirical model for the temperature derivative of the refractive index was proposed for the ZGP crystal. In it, the temperature dependences of the band gap width ( $E_g$ ) and the thermal expansion coefficient (TEC) of the medium make a decisive contribution to  $dn_i/dT$ . But this model determines the character of the dependence only for the first-order derivative. This is not enough for some tasks.

Figure 7 shows the dependence of  $dn_i/dT$  versus wavelength, calculated with data from various publications at room temperature. Solid lines correspond to  $dn_x/dT$ , and dotted lines correspond to  $dn_z/dT$ . The experimental data from the first work [22] are also marked with dots there ( $dn_x/dT$ —green squares and  $dn_z/dT$ —red circles). Given the general nature of the dependencies near the left border of the transparency range, they differ significantly in the long-wavelength part of the crystal transparency range. There is also a significant quantitative difference among all the results.

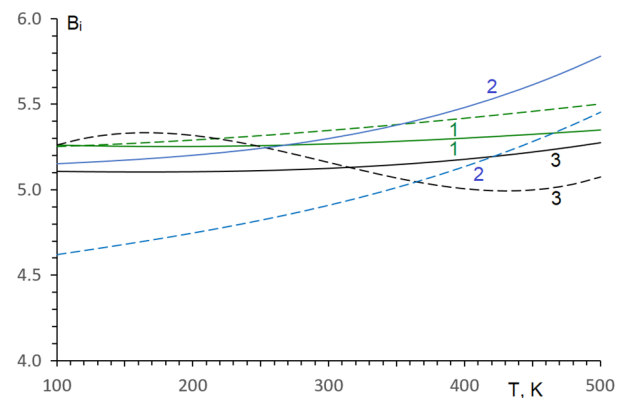
Figure 8 shows the dependencies for the coefficients  $A_i, B_i, C_i, D_i$  of the Sellmeier Equations (1) and (2) versus temperature with data from various publications. Solid lines correspond to  $n_o = n_x$ , and dotted lines correspond to  $n_e = n_z$ . All coefficients have comparable values, and the ratios between them for  $n_x$  and  $n_z$  are generally the same. But the nature of the change for the coefficients  $A_i, B_i$  and  $C_i$  is significantly different. Only in [49] the temperature dependence for the  $D_i$  coefficient was determined. But this is a very small dependency. In other works, the value of this coefficient is determined by a constant.



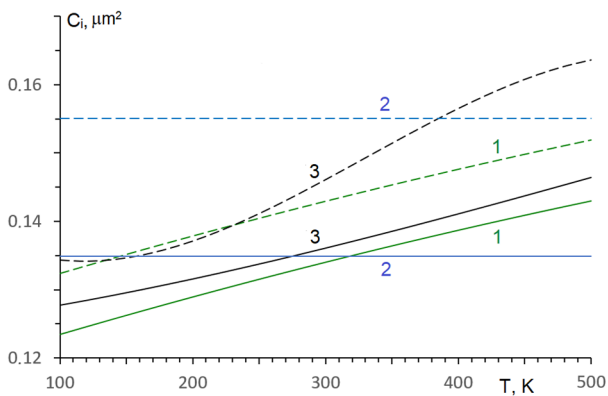
**Figure 7.** Dependencies for  $dn_i/dT$  versus wavelength with different data from publications: 1—[47], 2—[43], 3—[35], 4—[36], 5—[49].



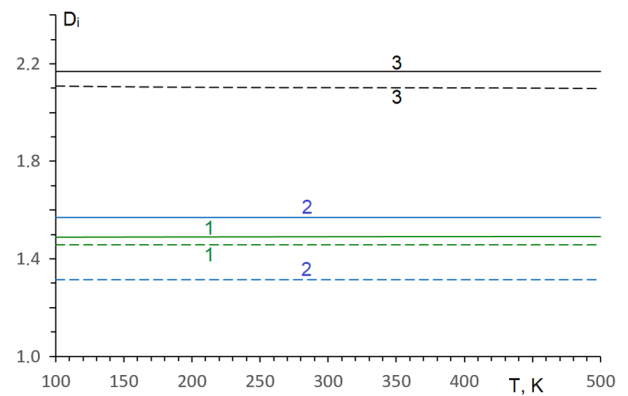
(a)  $A_i$



(b)  $B_i$



(c)  $C_i$



(d)  $D_i$

**Figure 8.** Temperature dependence for coefficients of Sellmeier equations from different publications: 1—[36], 2—[47], 3—[49].

In [49], the nature of the temperature dependences of all coefficients is not explained. It can be assumed that the data for the temperature dependence of the Sellmeier equations coefficients in [49] were obtained by mathematical formalism under approximation. A comparison of the results in Figure 8 shows that the approximation problem does not have a single solution. A single consistent methodology for processing measurement results is required.

It is necessary to note the work [64], in which the birefringence dispersion was measured by the interference method at various temperatures in the crystal transparency range.

Not enough attention is paid to this work. A good agreement with its results can be obtained only when using the equations from [49]. The corresponding dependencies are shown in Figure 9. The dots show the measurement results from [55,64], and the solid lines show the results of calculations using equations [49].

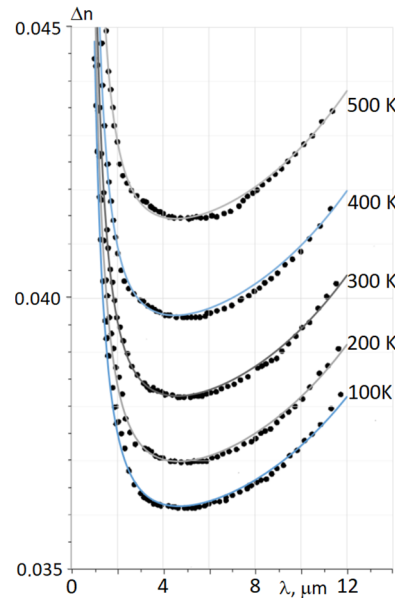


**Figure 9.** Dependencies of  $\Delta n(\lambda)$  versus wavelength for different temperature of the crystal.

With the available data for the values of  $n_i(\lambda)$  and  $dn_i(\lambda)/dT$ , it is possible to determine the values of temperature widths of phase matching for all frequency conversion processes, the possibility of temperature tunability of the wavelength in the OPO, and the wavelengths for a temperature-critical regime. Temperature derivatives of the first order play a decisive role in this regime. In a form similar to Figure 5, the distributions for the values of the temperature widths of phase matching from the radiation wavelengths calculated with first-order derivatives  $dn_i(\lambda)/dT$  can be given. All values are determined along the directions of phase matching (Figure 5a). Figure 10 shows the distributions of  $2\Delta T(\lambda_1, \lambda_2)$  (the coefficient 2 is introduced, since in the general case the values of positive and negative temperature derangement differ significantly) obtained with data for the dispersion of refractive indices  $n_i(\lambda)$  from [46], and for  $dn_i(\lambda)/dT$  from [43]. It follows from them that the smallest phase-matching temperature band width takes place for SHG at the edges of the transparency range. In this area, the character of the dependence of efficiency on temperature exactly corresponds to  $\text{sinc}^2(x)$ . This character of the dependence will make it possible to organize the temperature adjustment of the wavelength in OPO [49,51,65].

In the wavelength range for SHG at 6  $\mu\text{m}$ , the conversion process is temperature critical, but the temperature width exceeds 100  $^\circ\text{C}\cdot\text{cm}$ . This takes place for both the *eeo* and *oeo* types of interaction. There is an abnormal region at SHG with wavelengths of  $\lambda_2 = 1.2 \mu\text{m}$  and  $\lambda_1 = 10\text{--}12 \mu\text{m}$ . There are small values of temperature phase-matching bandwidth near this area. But in a narrow area of this wavelength range, the values of temperature widths exceed 150  $^\circ\text{C}\cdot\text{cm}$ .

The dependence of the wave-vectors mismatch on the parameters is determined by the Taylor series

$$\Delta k(p) = \Delta k_0 + \frac{d\Delta k}{dp} \Delta p + \frac{1}{2} \frac{d^2\Delta k}{dp^2} \Delta p^2 + \dots + \frac{1}{m!} \frac{d^m \Delta k}{dp^m} \Delta p^m \tag{4}$$

where  $p = \varphi, \theta, \lambda, T$ .

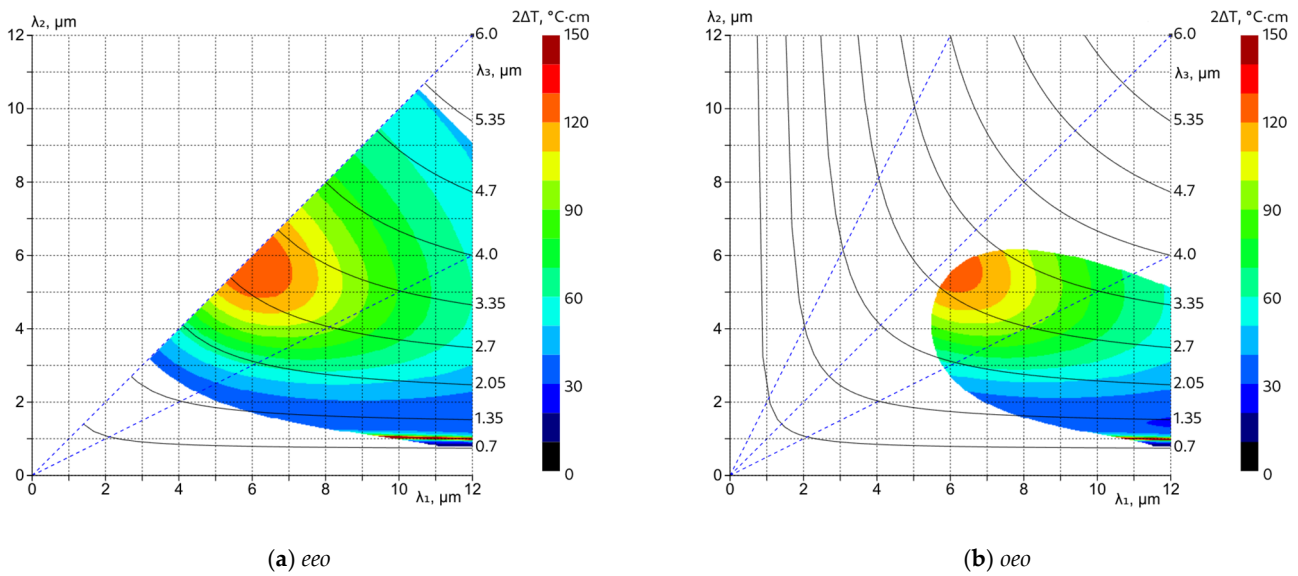


**Figure 10.** Results for temperature bandwidth along phase-matching direction with data for  $n_i(\lambda)$  from [46] and  $dn_i(\lambda)/dT$  from [43].

Critical phase matching takes place when  $d\Delta k/dp \neq 0$ , and noncritical for  $d\Delta k/dp = 0$ . The phase-matching width (at level 0.5) for a critical process is

$$\Delta p \cdot L = 0.886\pi / (d\Delta k/dp) \tag{5}$$

and for a non-critical second-order process

$$\Delta p \cdot \sqrt{L} = \sqrt{1.772\pi / (d^2\Delta k/dp^2)} \tag{6}$$

The results of Figure 5 show that all derivatives of  $dn_i(\lambda)/dT$  have large values. But their difference for some processes in the directions of phase matching is zero. It follows from this that temperature non-critical phase matching (TNCPhM) takes place. For the *eeo* type of interaction, the directions of the TNCPhM are determined from the condition [66]

$$\frac{d\Delta k_{eeo}(\theta_{pm})}{dT} = 2\pi \left[ \frac{1}{\lambda_3} \frac{dn_{3,o}}{dT} - \frac{1}{\lambda_2} \frac{dn_{2,e}(\theta_{pm})}{dT} - \frac{1}{\lambda_1} \frac{dn_{1,e}(\theta_{pm})}{dT} \right] = 0 \tag{7}$$

and for the *oeo* type

$$\frac{d\Delta k_{oeo}(\theta_{pm})}{dT} = 2\pi \left[ \frac{1}{\lambda_3} \frac{dn_{3,o}}{dT} - \frac{1}{\lambda_2} \frac{dn_{2,e}(\theta_{pm})}{dT} - \frac{1}{\lambda_1} \frac{dn_{1,o}}{dT} \right] = 0 \tag{8}$$

The article [43] was the first to establish the fact of the possible implementation of the TNCPhM regime in a uniaxial ZGP crystal for some frequency conversion processes. But it provides data only for first-order derivatives. This does not allow us to determine the full value of  $2\Delta T$ .

The application of first-order derivatives in calculations makes it possible to determine the temperature width of the temperature-critical process and the directions of the TNCPhM. To determine the full temperature widths, more accurate data on the temperature dependence of the refractive indices are necessary, for example, with higher-order derivatives. For this purpose, data from [49] can be used, in which the main coefficients of the Sellmeier equation are determined with a degree up to  $T^3$ . Figure 11 shows distributions similar to Figure 10 obtained with data for  $n_i(\lambda)$  and  $dn_i(\lambda)/dT$  from [49].

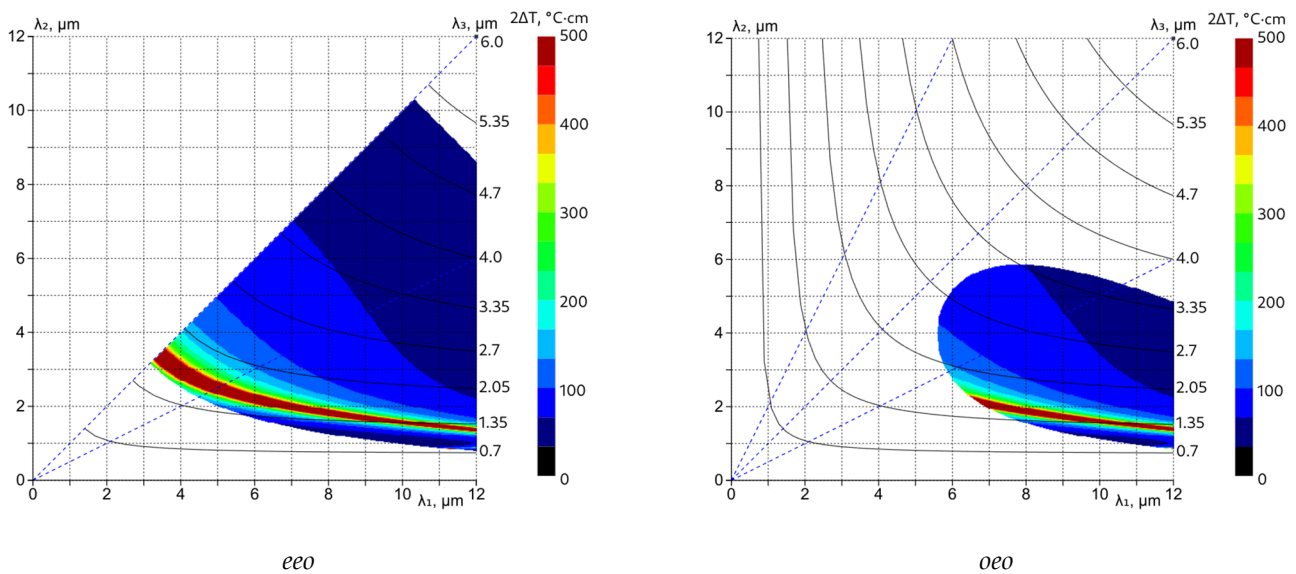


**Figure 11.** Results for temperature bandwidth along phase-matching direction with data for  $n_i(\lambda)$ , and  $dn_i(\lambda)/dT$  from [49].

In general, the values of the wavelengths of the TNCPhM area in Figures 10 and 11 are consistent. The results of Figure 11 show that the TNCPhM regime for two types of interaction can be obtained in a sufficiently large wavelength range for both SHG and SFG.

It should be noted that from calculation with data from [49], the temperature non-critical phase matching for generation of the second harmonic with the *eeo* type of interaction takes place at a wavelength of 3.4  $\mu\text{m}$ . This is inconsistent with the results of [36,38,44], which show the dependences of the phase-matching angle for SHG on the wavelength at different temperatures, calculated on the basis of the values  $n_i(\lambda)$  and  $dn_i(\lambda)/dT$  measured by the authors. The phase-matching angle practically does not change in the temperature range from  $-200\text{ }^\circ\text{C}$  to  $400\text{ }^\circ\text{C}$  at a wavelength of about 4.5  $\mu\text{m}$ . This raises the question of the need to refine the data for  $dn_i/dT$ .

The results of Figure 11 show that a temperature non-critical process can be obtained for SFG. This can be represented as a dependence of the temperature derivative for the phase-matching angle  $d\theta_{pm}/dT$  from the wavelength. Figure 12 shows the dependence of  $d\theta_{pm}/dT$  versus the wavelength  $\lambda_2$  at SFG with  $\lambda_1 = 10.3\text{ }\mu\text{m}$  for the *eeo* type of interaction. At a wavelength of  $\lambda_2 = 1.65\text{ }\mu\text{m}$ , the value of  $d\theta_{pm}/dT = 0$ . This corresponds to the TNCPhM regime.

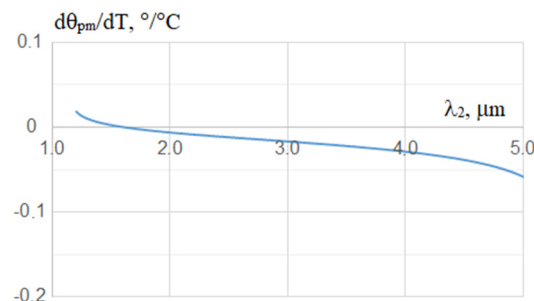
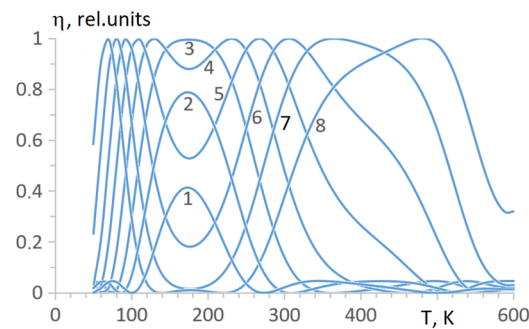


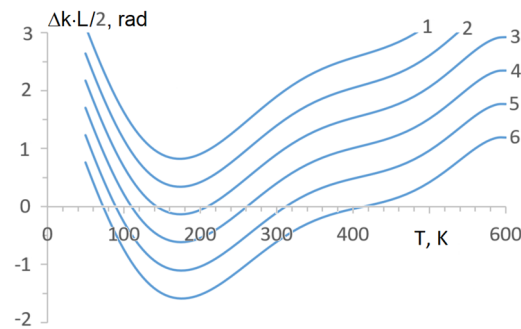
**Figure 12.** Temperature derivative for angle of phase matching for SFG versus wavelength  $\lambda_2$  for *eeo* type of interaction.

The character of the radiation intensity dependency from temperature is determined by the contribution of temperature derivatives of refractive indices of various orders, the values of which are commensurate. Figure 13 shows the dependences of the relative efficiency of the conversion versus the temperature for SHG at a wavelength of 3.407  $\mu\text{m}$

with the *eeo* type of interaction at different cut-off angles in a 50 mm-length crystal. The nature of their change corresponds to the transition from a critical to a non-critical process, similar to the dependencies on changes of the angle and wavelength of radiation. The transition from curve 1 to curve 3 in Figure 13a corresponds to the achievement of phase matching at a temperature  $T = 180$  K. With a further increase in the angle (the transition from curve 3 to curve 8), two extremes are formed at different temperatures of crystal. The difference in the distribution of the two dependences of  $I_2(T)$  is determined by the nature of the change in refractive indices from the temperature. This is shown by the dependence of the phase detuning  $\Delta k \cdot L/2$  from temperature, shown in Figure 13b.



(a) relative efficiency versus temperature



(b) the wave-vectors mismatch versus temperature

**Figure 13.** Dependencies of relative efficiency (a) and wave-vectors mismatch (b) versus temperature for *eeo* type at different angles: 1—69.95°, 2—70.0°, 3—70.05°, 4—70.1°, 5—70.15°, 6—70.2°, 7—70.25°, 8—70.3°.

There are cut-off angles at which there is a significant difference in the nature of the distribution of the left and right parts of the dependence of the conversion efficiency. Figure 14 shows the dependence of the conversion efficiency on the temperature at SHG with a wavelength of 3.358  $\mu\text{m}$  for the *eeo* type of interaction in a 50 mm-length crystal. The temperature width of the right side of the distribution is  $\Delta T = 320$  °C.

The temperature dependence versus the crystal length is not simple for various processes (see (5) and (6)). For a critical process, the phase-matching width is inversely proportional to the length of the crystal. For non-critical derivatives determined by the action of only second-order derivatives, it is inversely proportional to  $\sqrt{2}$ . Figure 15 shows the dependences of the relative conversion efficiency for SHG with *eeo* type of interaction at a wavelength of 3.407  $\mu\text{m}$  with a crystal length of 4 mm (curve 1) and 2 mm (curve 2). The ratio of temperature widths for the two crystal lengths is 1.87, differing by a factor of 2. This shows that a commensurate contribution to the value of  $\Delta T$  is made by derivatives of the first and higher orders. It follows that in the general case of temperature-noncritical processes, it is impossible to determine the value of the temperature bandwidth of the phase matching per unit length of the crystal.

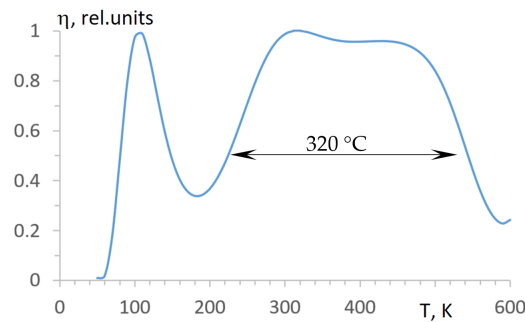


**Figure 14.** The relative efficiency versus temperature for *eeo* type of interaction versus temperature at  $\lambda_1 = \lambda_2 = 3.358 \mu\text{m}$ ,  $\theta = 71.99^\circ$ .

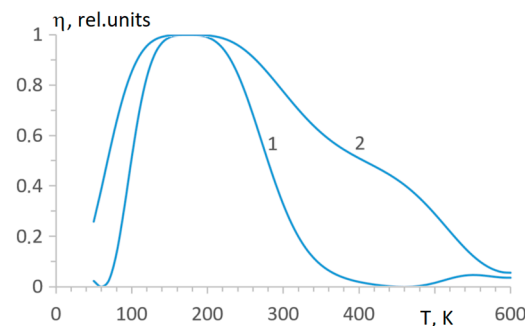


**Figure 15.** Relative efficiency for SHG versus temperature at  $\lambda_1 = 3.407 \mu\text{m}$ ,  $\theta_{\text{pm}} = 70.12^\circ$  for different lengths of crystal: 1—4 mm, 2—2 mm.

For any frequency conversion process in biaxial crystals, temperature-noncritical phase matching can be obtained in a sufficiently large wavelength range [66]. It is possible for uniaxial crystals at fixed wavelengths. In the general case, the TNCPm mode can be obtained at not one, but several, fixed wavelengths. This follows from the fact that the condition  $d\Delta k_i/dT = 0$  with a commensurate contribution of derivatives of different orders has several roots. They correspond to different values of radiation wavelengths. All this is determined by the character of the refractive-indices temperature dependence.

All these questions require separate research. The above calculation results set the task of obtaining experimental confirmations.

## 5. Conclusions

The paper presents data on the physical parameters of the ZGP crystal, which have been obtained over the past 20 years of this research medium. The development of growth technology and post-growth treatment made it possible to significantly reduce the absorption, and obtain good optical quality and high damage thresholds in various modes. This makes it possible to use the crystal to solve a wide range of problems of generating radiation in the mid-IR range.

The paper shows the functional capabilities of the ZGP crystal for various frequency conversion tasks—both sum-frequency generation and parametric-frequency conversion with a large range of wavelength tuning or a large spectral width of radiation.

The question about the temperature dependence for values of the refractive indices is very relevant. For the first time, some new data show that temperature-noncritical phase matching is possible in the ZGP crystal at SHG, SFG, DFG and OPO with an abnormally large temperature bandwidth. On the one hand, this removes the question on the necessary thermal stabilization of the crystal and reduces the effect of thermal self-interaction on the conversion process. On the other hand, this does not make it possible to organize a temperature tuning of the radiation wavelength in OPO. It is necessary to execute the corresponding experimental investigations.

The difference in the obtained calculation results shows that it is necessary to conduct a comparison analysis of the physical parameters of the crystal that obtained with different growth technologies and post-grown processing. It is necessary to determine the most reliable data that are necessary when executing the research into and design of the frequency converters.

**Author Contributions:** Conceptualization, investigation, software and calculations, writing—review and editing, S.G.G.; software and calculations, I.A.M. All authors have read and agreed to the published version of the manuscript.

**Funding:** This research received no external funding.

**Institutional Review Board Statement:** Not applicable.

**Informed Consent Statement:** Not applicable.

**Data Availability Statement:** Data are contained within the article.

**Conflicts of Interest:** The authors declare no conflicts of interest.

## References

1. Vodopyanov, K.L. Chapter 7: Mid-IR Applications. In *Laser-Based Mid-Infrared Sources and Applications*; John Wiley & Sons: Hoboken, NJ, USA, 2020; pp. 247–286.
2. Ebrahim-Zadeh, M.; Sorokina, I.T. *Mid-Infrared Coherent Sources and Applications*; Springer: Berlin/Heidelberg, Germany, 2008.
3. Tittel, F.K.; Richter, D.; Fried, A. Mid-Infrared laser applications in spectroscopy. In *Solid-State Mid-Infrared Laser Sources*; Sorokina, I.T., Vodopyanov, K.L., Eds.; Springer: Berlin/Heidelberg, Germany, 2003; pp. 458–529.
4. Ozaki, Y. Infrared Spectroscopy—Mid-infrared, near-infrared, and far-infrared/terahertz spectroscopy: Reviews. *Anal. Sci.* **2021**, *37*, 1193–1212. [[CrossRef](#)] [[PubMed](#)]
5. Jean, B.; Bende, T. Mid-IR laser applications in medicine. In *Solid-State Mid-Infrared Laser Sources*; Sorokina, I.T., Vodopyanov, K.L., Eds.; Springer: Berlin/Heidelberg, Germany, 2003; pp. 530–565.
6. Kazarian, S.G.; Chan, K.L. ATR-FTIR spectroscopic imaging: Recent advances and applications to biological systems. *Analyst* **2013**, *138*, 1940–1951. [[CrossRef](#)] [[PubMed](#)]
7. Fujimoto, J.G. Optical coherence tomography for ultrahigh resolution in vivo imaging. *Nat. Biotechnol.* **2003**, *21*, 1361–1367. [[CrossRef](#)] [[PubMed](#)]
8. López-Lorente, Á.I.; Mizaikoff, B. Mid-infrared spectroscopy for protein analysis: Potential and challenges. *Anal. Bioanal. Chem.* **2016**, *408*, 2875–2889. [[CrossRef](#)] [[PubMed](#)]
9. Sabbah, S.; Harig, R.; Rusch, P.; Eichmann, J.; Keens, A.; Gerhard, J.H. Remote sensing of gases by hyperspectral imaging: System performance and measurements. *Opt. Eng.* **2012**, *51*, 111717. [[CrossRef](#)]
10. Hodgkinson, J.; Tatam, R.P. Optical gas sensing: A review. *Meas. Sci. Technol.* **2013**, *24*, 012004. [[CrossRef](#)]
11. Du, Z.; Zhang, S.; Li, J.; Gao, N.; Tong, K. Mid-Infrared tunable laser-based broadband fingerprint absorption spectroscopy for trace gas sensing: A review. *Appl. Sci.* **2019**, *9*, 338. [[CrossRef](#)]
12. Li, J.; Yu, Z.; Du, Z.; Ji, Y.; Liu, C. Standoff chemical detection using laser absorption spectroscopy: A review. *Remote Sens.* **2020**, *12*, 2771. [[CrossRef](#)]
13. Casadio, F.; Toniolo, L. The analysis of polychrome works of art: 40 years of infrared spectroscopic investigations. *J. Cult. Herit.* **2001**, *2*, 71–78. [[CrossRef](#)]
14. Mazzeo, R. (Ed.) *Analytical Chemistry for Cultural Heritage*; Springer: Berlin/Heidelberg, Germany, 2016; Volume 374, 370p.
15. Tinti, A.; Tugnoli, V.; Bonora, S.; Francioso, O. Recent applications of vibrational mid-Infrared (IR) spectroscopy for studying soil components: A review. *J. Cent. Eur. Agric.* **2015**, *16*, 1–22. [[CrossRef](#)]
16. Petrov, V. Parametric down-conversion devices: The coverage of the mid-infrared spectral range by solid-state laser sources. *Optic. Mater.* **2012**, *34*, 536–554. [[CrossRef](#)]
17. Petrov, V. Frequency down-conversion of solid-state laser sources to the mid-infrared spectral range using non-oxide nonlinear crystals. *Prog. Quantum Electron.* **2015**, *42*, 1–106. [[CrossRef](#)]
18. Ebrahim-Zadeh, M.; Chaitanya Kumar, S.; Esteban-Martin, A.; Samanta, G.K. Breakthroughs in photonics 2012: Breakthroughs in optical parametric oscillators. *IEEE Photon. J.* **2013**, *5*, 0700105. [[CrossRef](#)]
19. Schunemann, P.G. Improved NLO crystals for mid-IR laser applications. *Proc. SPIE* **2007**, *6455*, 64550R. [[CrossRef](#)]
20. Schunemann, P.G.; Zawilski, K.T.; Pomeranz, L.A.; Creeden, D.J.; Budni, P.A. Advances in nonlinear optical crystals for mid-infrared coherent sources. *J. Opt. Soc. Am. B* **2016**, *33*, D36–D43. [[CrossRef](#)]
21. Goryunova, N.A. *Chemistry of Diamond-Like Semiconductors*; Anderson, J.C., Ed.; The MIT Press: Cambridge, MA, USA, 1965; 242p.
22. Boyd, G.D.; Buehler, E.; Storz, F.G. Linear and nonlinear optical properties of ZnGeP<sub>2</sub> and CdSe. *Appl. Phys. Lett.* **1971**, *18*, 301–304. [[CrossRef](#)]
23. Nikogosyan, D.N. *Nonlinear Optical Crystals*; Springer: Berlin/Heidelberg, Germany, 2005; 427p. [[CrossRef](#)]

24. Available online: <http://fc.gpi.ru> (accessed on 5 March 2024).
25. Hobgood, H.M.; Henningsen, T.; Thomas, R.N.; Hopkins, R.H.; Ohmer, M.C.; Mitchel, W.C.; Hopkins, F.K. ZnGeP<sub>2</sub> grown by the liquid encapsulated Czochralski method. *J. Appl. Phys.* **1993**, *73*, 4030–4036. [[CrossRef](#)]
26. Mason, P.D.; Jackson, D.J.; Gorton, E.K. CO<sub>2</sub> laser frequency doubling in ZnGeP<sub>2</sub>. *Opt. Commun.* **1994**, *110*, 163–166. [[CrossRef](#)]
27. Alford, W.J.; Smith, A.V. Wavelength variation of the second-order nonlinear coefficients of KNbO<sub>3</sub>, KTiOPO<sub>4</sub>, KTiOAsO<sub>4</sub>, LiNbO<sub>3</sub>, LiIO<sub>3</sub>, β-BaB<sub>2</sub>O<sub>4</sub>, KH<sub>2</sub>PO<sub>4</sub>, and LiB<sub>3</sub>O<sub>5</sub> crystals: A test of Miller wavelength scaling. *J. Opt. Soc. Am. B* **2001**, *18*, 524–533. [[CrossRef](#)]
28. Verozubova, G.A.; Okunev, A.O.; Gribenyukov, A.I.; Trofimov, A.Y.; Trukhanov, E.M.; Kolesnikov, A.V. Growth and defect structure of ZnGeP<sub>2</sub> crystals. *J. Cryst. Growth* **2010**, *312*, 1122–1126. [[CrossRef](#)]
29. Andreev, Y.M.; Butuzov, V.V.; Verozubova, G.A.; Gribenyukov, A.I.; Davydov, S.V.; Zakharov, V.P. Generation of the second harmonic of pulsed CO<sub>2</sub>-laser radiation in AgGaSe<sub>2</sub> and ZnGeP<sub>2</sub> single crystals. *Laser Phys.* **1995**, *5*, 1014–1019.
30. Ketteridge, P.A.; Budni, P.A.; Schunemann, P.G.; Lemons, M.; Pollack, T.M.; Chicklis, E.P. Tunable all solid state average power ZGP OPO at 2.7 and 8.5 microns. *Advanced Solid-State Lasers. OSA Trends Opt. Photonics Ser.* **1998**, *19*, 233–235. [[CrossRef](#)]
31. Medvedkin, G.A.; Voevodin, V.G. Magnetic and optical phenomena in nonlinear optical crystals ZnGeP<sub>2</sub> and CdGeP<sub>2</sub>. *J. Opt. Soc. Am. B* **2005**, *22*, 1884–1898. [[CrossRef](#)]
32. Yudin, N.; Antipov, O.; Eranov, I.; Gribenyukov, A.; Verozubova, G.; Lei, Z.; Yang, C. Laser-induced damage threshold of single crystal ZnGeP<sub>2</sub> at 2.1 μm: The effect of crystal lattice quality at various pulse widths and repetition rates. *Crystals* **2022**, *12*, 652. [[CrossRef](#)]
33. Yudin, N.; Dyomin, V.; Gribenyukov, A.; Antipov, O.; Khudoley, A.; Kinyaevskiy, I.O.; Baalbaki, H. Physical and Technological Aspects of Laser-Induced Damage of ZGP Single Crystals under Periodically Pulsed Laser Irradiation at 2.1 μm. *Photonics* **2023**, *10*, 1364. [[CrossRef](#)]
34. Bhar, G.C. Refractive index interpolation in phase-matching. *Appl. Opt.* **1976**, *15*, 305–307. [[CrossRef](#)] [[PubMed](#)]
35. Bhar, G.C.; Ghosh, G. Temperature-dependent Sellmeier coefficients and coherence lengths for some chalcopyrite crystals. *J. Opt. Soc. Am.* **1979**, *69*, 730–733. [[CrossRef](#)]
36. Bhar, G.C.; Ghosh, G. Temperature dependent phase-matched nonlinear optical devices using CdSe and ZnGeP<sub>2</sub>. *IEEE J. Quantum Electron.* **1980**, *16*, 838–843. [[CrossRef](#)]
37. Kato, K. Second-harmonic and sum-frequency generation in ZnGeP<sub>2</sub>. *Appl. Opt.* **1997**, *36*, 2506–2510. [[CrossRef](#)]
38. Ghosh, G. Sellmeier coefficients for the birefringence and refractive indices of ZnGeP<sub>2</sub> nonlinear crystal at different temperatures. *Appl. Opt.* **1998**, *37*, 1205–1212. [[CrossRef](#)]
39. Barnes, N.P.; Murray, K.E.; Jani, M.G.; Schunemann, P.G.; Pollak, T.M. ZnGeP<sub>2</sub> parametric amplifier. *J. Opt. Soc. Am. B* **1998**, *15*, 232–238. [[CrossRef](#)]
40. Zakharov, S.V.; Negin, A.E.; Filippov, P.G.; Zhilis, E.F. Sellmeier equation and conversion of the radiation of a repetitively pulsed tunable TEA CO<sub>2</sub> laser into the second harmonic in a ZnGeP<sub>2</sub> crystal. *Quantum Electron.* **1999**, *29*, 806–810. [[CrossRef](#)]
41. Madarasz, F.L.; Dimmock, J.O.; Deitz, N.; Bachmann, K.J. Sellmeier parameters for ZnGeP<sub>2</sub> and GaP. *J. Appl. Phys.* **2000**, *87*, 1564–1565; Erratum in *J. Appl. Phys.* **2000**, *87*, 7597. [[CrossRef](#)]
42. Zelmon, D.E.; Hanning, E.A.; Schunemann, P.G. Refractive-index measurements and Sellmeier coefficients for zinc germanium phosphide from 2 to 9 μm with implications for phase matching in optical frequency-conversion devices. *J. Opt. Soc. Am. B* **2001**, *18*, 1307–1310. [[CrossRef](#)]
43. Kato, K.; Takaoka, E.; Umemura, N. New Sellmeier and thermo-optic dispersion formulas for ZnGeP<sub>2</sub>. In Proceedings of the Conference on Lasers and Electro-Optics/Quantum Electronics and Laser Science Conference, Baltimore, MD, USA, 1–6 June 2003; p. NCTuM17.
44. Das, S.; Bhar, G.C.; Gangopadhyay, S.; Ghosh, C. Linear and nonlinear optical properties of ZnGeP<sub>2</sub> crystal for infrared laser device applications: Revisited. *Appl. Opt.* **2003**, *42*, 4335–4340. [[CrossRef](#)] [[PubMed](#)]
45. Kumbhakar, P.; Kobayashi, T.; Bhar, G.C. Sellmeier dispersion for phase-matched terahertz generation in ZnGeP<sub>2</sub>. *Appl. Opt.* **2004**, *43*, 3324–3328. [[CrossRef](#)]
46. Kato, K.; Umemura, N.; Okamoto, T.; Mikami, T. Modified Sellmeier equations for ZnGeP<sub>2</sub> in the 0.97–1640 μm range. *Proc. SPIE* **2011**, 7917, 79171V. [[CrossRef](#)]
47. Guha, S. Updated temperature dependent Sellmeier equations for ZnGeP<sub>2</sub> crystals. *Proc. SPIE* **2019**, 10902, 1090210. [[CrossRef](#)]
48. Ionin, A.A.; Kinyaevskiy, I.O.; Klimachev, Y.M.; Kozlov, A.Y.; Sagitova, A.M.; Seleznev, L.V.; Andreev, Y.M. Temperature phase-matching tuning of nonlinear ZnGeP<sub>2</sub> crystal for frequency conversion under noncritical spectral phase-matching. *Infrared Phys. Technol.* **2019**, *102*, 103009. [[CrossRef](#)]
49. Wang, H.; Tian, J.; Zhao, L.; Li, Z.; Tan, R. ZnGeP<sub>2</sub> optical parametric oscillator with wide temperature tuning. *Opt. Commun.* **2023**, *542*, 129584. [[CrossRef](#)]
50. Bhar, G.C.; Samanta, L.K.; Ghosh, D.K. Tunable parametric ZnGeP<sub>2</sub> crystal oscillator. *Sov. J. Quantum Electron.* **1987**, *17*, 860–862. [[CrossRef](#)]
51. Andreev, Y.M.; Voevodin, V.G.; Gribenyukov, A.I.; Zyryanov, O.Y.; Ippolitov, I.I.; Morozov, A.N.; Khmel'nitskiĭ, G.S. Efficient generation of the second harmonic of tunable CO<sub>2</sub> laser radiation in ZnGeP<sub>2</sub>. *Sov. J. Quantum Electron.* **1984**, *14*, 1021–1022. [[CrossRef](#)]

52. Boyd, G.D.; Buehler, E.; Storz, F.G.; Wernick, J. Linear and nonlinear optical properties of ternary A<sup>II</sup>B<sup>IV</sup>C<sup>2V</sup> chalcopyrite semiconductors. *IEEE J. Quant. Electron.* **1972**, *8*, 419–426. [[CrossRef](#)]
53. Eichhorn, M.; Stuppler, G.; Schellhorn, M.; Zawilski, K.T.; Schunemann, P.G. Gaussian- versus flat-top-pumping of a mid-IR ZGP RISTRA OPO. *Appl. Phys. B* **2012**, *108*, 109–115. [[CrossRef](#)]
54. Ray, B.; Payne, A.J.; Burrell, G.J. Preparation and some physical properties of ZnGeP<sub>2</sub>. *Phys. Stat. Solidi (b)* **1969**, *35*, 197–204. [[CrossRef](#)]
55. Fischer, D.W.; Ohmer, M.C. Temperature dependence of ZnGeP<sub>2</sub> birefringence using polarized light interference. *J. Appl. Phys.* **1997**, *81*, 425–431. [[CrossRef](#)]
56. Grigoreva, V.S.; Prochukhan, V.D.; Rud, Y.V.; Yakovenko, A.A. Some electrical properties of high-resistance ZnGeP<sub>2</sub> single crystals. *Phys. Stat. Solidi (a)* **2006**, *17*, K69–K74. [[CrossRef](#)]
57. Medvedkin, G.A. Optical dichroism in ZnGeP<sub>2</sub> crystals at deep levels. *J. Opt. Soc. Am. B* **2022**, *39*, 851–858. [[CrossRef](#)]
58. Wang, Z.; Mao, M.; Wu, H.; Ni, Y.; Huang, C.; Cheng, X. Study on annealing of infrared nonlinear optical crystal ZnGeP<sub>2</sub>. *J. Cryst. Growth* **2012**, *359*, 11–14. [[CrossRef](#)]
59. Cordell, J.J.; Pucurimay, L.; Schnepf, R.R.; Levy-Wendt, B.L.; Toney, M.F.; Tucker, G.J.; Tamboli, A.C. Simulation and characterization of cation disorder in ZnGeP<sub>2</sub>. *J. Mater. Res.* **2022**, *37*, 1986–1996. [[CrossRef](#)]
60. Voevodin, V.I.; Brudnyi, V.N.; Sarkisov, Y.S.; Su, X.; Sarkisov, S.Y. Electrical relaxation and transport properties of ZnGeP<sub>2</sub> and 4H-SiC crystals measured with terahertz spectroscopy. *Photonics* **2023**, *10*, 827. [[CrossRef](#)]
61. Sooriyagoda, R.; Piyathilaka, H.P.; Zawilski, K.T.; Schunemann, P.G.; Bristow, A.D. Carrier transport and electron–lattice interactions of nonlinear optical crystals CdGeP<sub>2</sub>, ZnGeP<sub>2</sub>, and CdSiP<sub>2</sub>. *J. Opt. Soc. Am. B* **2021**, *38*, 769–775. [[CrossRef](#)]
62. Andreev, Y.M.; Arapov, Y.D.; Grechin, S.G.; Kasyanov, I.V.; Nikolaev, P.P. Functional possibilities of nonlinear crystals for frequency conversion: Uniaxial crystals. *Quantum Electron.* **2016**, *46*, 33–38. [[CrossRef](#)]
63. Bhar, G.C.; Ghosh, G.C. Dispersion of thermo-optic coefficients in nonlinear crystals. *Appl. Opt.* **1980**, *19*, 1029–1031. [[CrossRef](#)] [[PubMed](#)]
64. Fischer, D.W.; Ohmer, M.C.; Schunemann, P.G.; Pollak, T.M. Direct measurement of ZnGeP<sub>2</sub> birefringence from 0.66 to 12.2 μm using polarized light interference. *J. Appl. Phys.* **1995**, *77*, 5942. [[CrossRef](#)]
65. Bhar, G.C.; Das, S.; Chatterjee, U.; Vodopyanov, K.L. Temperature-tunable second-harmonic generation in zinc germanium phosphide. *Appl. Phys. Lett.* **1989**, *54*, 313–314. [[CrossRef](#)]
66. Grechin, S.G.; Dmitriev, V.G.; Dyakov, V.A.; Pryalkin, V.I. Dispersion of the temperature-noncritical frequency conversion and birefringence in biaxial optical crystals. *Quantum Electron.* **2004**, *34*, 461–466. [[CrossRef](#)]

**Disclaimer/Publisher’s Note:** The statements, opinions and data contained in all publications are solely those of the individual author(s) and contributor(s) and not of MDPI and/or the editor(s). MDPI and/or the editor(s) disclaim responsibility for any injury to people or property resulting from any ideas, methods, instructions or products referred to in the content.